



# Tin and Tin Compound Materials as Anodes in Lithium-Ion and Sodium-Ion Batteries: A Review

Haoyi Mou, Wei Xiao\*, Chang Miao, Rui Li and Liming Yu

College of Chemistry and Environmental Engineering, Yangtze University, Jingzhou, China

Tin and tin compounds are perceived as promising next-generation lithium (sodium)-ion batteries anodes because of their high theoretical capacity, low cost and proper working potentials. However, their practical applications are severely hampered by huge volume changes during  $\text{Li}^+$  ( $\text{Na}^+$ ) insertion and extraction processes, which could lead to a vast irreversible capacity loss and short cycle life. The significance of morphology design and synergic effects-through combining compatible compounds and/or metals together-on electrochemical properties are analyzed to circumvent these problems. In this review, recent progress and understanding of tin and tin compounds used in lithium (sodium)-ion batteries have been summarized and related approaches to optimize electrochemical performance are also pointed out. Superiorities and intrinsic flaws of the above-mentioned materials that can affect electrochemical performance are discussed, aiming to provide a comprehensive understanding of tin and tin compounds in lithium(sodium)-ion batteries.

**Keywords:** tin, tin compound, anode, lithium-ion batteries, sodium-ion batteries

## OPEN ACCESS

### Edited by:

Xianwen Wu,  
Jishou University, China

### Reviewed by:

Yunjian Liu,  
Jiangsu University, China  
Lingjun Li,  
Changsha University of Science and  
Technology, China

### \*Correspondence:

Wei Xiao  
xwylyq2006@126.com

### Specialty section:

This article was submitted to  
Electrochemistry,  
a section of the journal  
Frontiers in Chemistry

**Received:** 29 December 2019

**Accepted:** 14 February 2020

**Published:** 19 March 2020

### Citation:

Mou H, Xiao W, Miao C, Li R and Yu L  
(2020) Tin and Tin Compound  
Materials as Anodes in Lithium-Ion  
and Sodium-Ion Batteries: A Review.  
*Front. Chem.* 8:141.  
doi: 10.3389/fchem.2020.00141

## INTRODUCTION

Since the commercialization of lithium-ion batteries (LIBs) by the Sony Corporation in 1991, LIBs are widely used in portable devices, electric vehicles and energy storage equipment for their benefits of having no memory effect, long cycle life and high energy density (Tarascon and Armand, 2010; Kim et al., 2012; Wang et al., 2019). With largely depleting lithium resources, the existing limited and unevenly distributed lithium reserves cannot meet the increasing demands of LIBs (there is an estimated 17 ppm in the earth's crust; Grosjean et al., 2012). Due to abundant sodium reserves (there is an estimated 23,000 ppm in the earth's crust), sodium-based batteries can be an attractive alternative. Traditional Na-S batteries require operating temperatures between 300 and 350°C to allow sufficient  $\text{Na}^+$  conductivity of  $\text{NaAl}_{11}\text{O}_{17}$ , but safety issues and energy loss from maintaining the operating temperature are inevitable (Wen et al., 2008; Xin et al., 2014; Kou et al., 2019). Motivated by the similar chemical properties of sodium and lithium, researchers have shifted their attention to ambient temperature sodium-ion batteries (SIBs), but lots of problems need to be addressed for the practical application of SIBs (Yabuuchi et al., 2014; Li et al., 2018; Wu L. et al., 2018; Liu Y. et al., 2019). The main issue is the larger radius size of  $\text{Na}^+$  (1.09 Å) compared with  $\text{Li}^+$  (0.74 Å), which brings about sluggish reaction kinetics with low capacity, poor rate capability, and short cycling life (Chevrier and Ceder, 2011; Xu et al., 2013; Li et al., 2018). Extensive studies have been carried out to understand the requirements of commercial SIBs, which are great choices for low cost and large-scale energy storage equipment required for intermittent renewable energy and smart grids (Palomares et al., 2012; Pan et al., 2013). Comparitively, the energy density of

LIBs cannot fully satisfy an increasingly growing need for electronic energy storage devices (Xiao et al., 2018; Fang et al., 2020). The present conventional anode in LIBs is graphite, which follows a intercalation/de-intercalation reaction pathway with a low theoretical capacity (378 mAh/g) and is electrochemically unfavorable for SIBs owing to the larger size of  $\text{Na}^+$  (Qian et al., 2014). Therefore, not all successful experiences from LIBs are viable to be applied in SIBs. Usually, graphene and non-graphitic carbon (like hard carbon and carbon black) are conventional anodes in SIBs. Additionally,  $\text{TiO}_2$ ,  $\text{Na}_2\text{Ti}_3\text{O}_7$ , Sn,  $\text{SnO}_2$ ,  $\text{SnS}_2$ , Sb, and P, etc. are potential anode materials for  $\text{Na}^+$  storage in SIB systems (Slater et al., 2013; Li et al., 2018; Guan et al., 2020). Thanks to a similar charging-discharging mechanism, tin-based anodes' alloying/dealloying reactions have attracted considerable attention because they are applicable to both LIBs and SIBs with a high theoretical capacity (Stevens and Dahn, 2000; Zhu et al., 2013). Environmental benignity, low costs, and lower operating potentials than graphite are also attractive features for tin and tin compounds, but they contain the following intrinsic defects (Fu et al., 2016). Tin and tin compounds as anodes in LIBs (SIBs) sustain colossal volume changes during  $\text{Li}^+$  ( $\text{Na}^+$ ) insertion and extraction processes, which leads to pulverization of the active materials as well as losing electrical contact with the collector (Zhang, 2011; Liu D. et al., 2019). Moreover, a continuously regenerated solid electrolyte interphase (SEI) layer between the electrode and electrolyte interface will consume extra lithium (sodium) ions, causing large irreversible capacity loss and poor cycle stability (Beaulieu et al., 2001). Last but not least, the electronic conductivity of  $\text{SnO}_2$  (0.1 S/m) and  $\text{SnS}_2$  (1 S/m) is much inferior to Sn ( $9.1 \times 10^6$  S/m) (Thangaraju and Kaliannan, 2000; Saadeddin et al., 2006; Nie et al., 2020). To cope with these problems, many measures have been taken and summarized as follows.

Firstly, according to comprehensive investigations nano-scale tin and tin compounds can alleviate the inter stress brought on by volume changes, to some extent, and can shorten the transfer paths of lithium (sodium) ions and electrons. Additionally, more reactive sites on the interface between electrodes and electrolytes are generated (Uchiyama et al., 2008; Park and Park, 2015; Park et al., 2018). The second method is to incorporate tin and tin compounds with one or more stress-accommodating phases that have can assure electronic conductivity, such as carbonaceous materials, metals and some transitional metal compounds (Kepler et al., 1999; Takamura et al., 1999). In 2005, Sony commercialized the first tin-based amorphous anode with the trademark "Nexelion" and this anode is composed of Sn, Co and C, where Co and C are identified as conductive and stress-releasing phases. According to Sony, Nexelion has a capacity of 900 mAh, which is 28 % higher than conventional graphite (700 mAh) at 0.2°C. Extensive investigations have been made to find a feasible and low-cost way to synthesize tin- and tin compound-based anodes with satisfactory physicochemical and electrochemical properties for both LIBs and SIBs at the same time. In this review, we focus on the recent progress of Sn,  $\text{SnO}_2$ , and  $\text{SnS}_2$  as anodes in LIBs and SIBs. This comprehensive review provides an in-depth account of the similarities and differences between Sn,  $\text{SnO}_2$ , and  $\text{SnS}_2$  as used in LIBs (SIBs) as well as clear

directions for the structure design and fabrication procedures regarding anode material syntheses in LIBs and SIBs.

## TIN AND TIN COMPOUNDS IN LIBs

### Sn-Based Composites

Sn has a high theoretical specific capacity of 993.4 mAh/g, according to the reversible reaction  $\text{Sn} + x\text{Li}^+ + xe^- \leftrightarrow \text{Li}_x\text{Sn}$  ( $0 \leq x \leq 4.4$ ) (Lee et al., 2003). However, huge volume changes and aggregation of Sn particles during the alloying/dealloying process are the main obstacles for practical applications (Beaulieu et al., 2001). Generally, carbonaceous materials and Sn-based intermetallics are believed to address these issues efficiently and largely improve the battery performance of Sn-based anode materials (Zhao et al., 2015; Ying and Han, 2017). Carbon materials, either acting as the support or coating, can effectively ease volume changes and aggregation of Sn particles and increase the overall conductivity, especially with graphene (Wen et al., 2016). Zhou et al. have reported a high-performance anode where tin nanoparticles are impregnated into nitrogen-doped graphene (Zhou et al., 2013a). The graphene coating can facilitate electron transport and prevent aggregation of tin particles. Add void spaces between graphene and tin nanoparticles avail the accommodation of volume changes. As a result, the final composite delivers a reversible capacity of 481 mAh/g at a current density of 100 mA/g.

Some Sn-based intermetallics have also been considered as a promising choice, such as Sn-Cu, Sn-Co, Sn-Sb, Sn-Bi, Sn-Se, Sn-Fe and Sn-Ni etc (Yang et al., 1999; Yoon et al., 2009; Xue et al., 2010; Dang et al., 2015; Qin et al., 2017). Among all these types of intermetallics, Sony's Nexelion-consisting of Sn, Co, and C-is the first commercialized tin-based anode, but the composition is not fully revealed. Hence, it is important to further investigate the role and mechanism of cobalt in the Sn-Co intermetallic system. In principle, cobalt is considered an inactive component used to buffer the volume changes. However, according to the systematic study of  $\text{Sn}_{1-x}\text{Co}_x$  ( $0 < x < 0.6$ ) and  $[\text{Sn}_{0.55}\text{Co}_{0.45}]_{1-y}\text{C}_y$  ( $0 < y < 0.5$ ) conducted by Dahn et al., the  $\text{Sn}_{1-x}\text{Co}_x$  system is amorphous when  $0.28 < x < 0.43$  and an amorphous structure can hold part of the capacity in place of alloying anodes in LIBs. In addition, cobalt does not form intermetallic Co-carbides which avoids the exclusion of crystalline tin, improving the cycle stability of the composite (Tamura et al., 2004; Dahn et al., 2006; Todd et al., 2007; Li et al., 2011).

Sn-Cu alloy is another extensively explored anode in LIBs, especially in the stable  $\text{Cu}_6\text{Sn}_5$  intermetallic phase. According to the detailed *in-situ* X-ray study of  $\text{Cu}_6\text{Sn}_5$  by Larcher and his coworker, the two reverse phase transitions of  $\text{Cu}_6\text{Sn}_5$  reacting with  $\text{Li}^+$  are listed as follows (Larcher et al., 2000):



As the Cu content in the Cu-Sn alloy increases, the final obtained product will significantly improve in cyclability, because Cu is used as an inactive buffering matrix to relieve the volume expansion. However it also results in a relatively lower discharge

capacity, for example, the theoretical discharge specific capacity of  $\text{Cu}_6\text{Sn}_5$  in LIBs is 584 mAh/g (Trahey et al., 2009). Core/shell  $\text{Cu}_6\text{Sn}_5@/\text{SnO}_2\text{-C}$  anode materials are prepared by boiling Sn and Cu powders in a sucrose solution with air, as reported by Hu's group, in which  $\text{Cu}_6\text{Sn}_5$  as an inert foundation replaces the electrochemically inactive Cu, SiC and Ni (Hu et al., 2015). As a consequence, the composite exhibits a high discharge specific capacity of 619 mAh/g at 1.0°C after 500 cycles, and SEM images before and after the first cycle show that the maximum volume change ratio decreases to 12.7%.

On the other hand, some Sn-based intermetallics with electrochemically active metals, like Sb, Bi, and Ge, have shown higher initial capacities and better electrochemical properties than the individual active materials, which is due to the different potentials vs.  $\text{Li}^+/\text{Li}$  of these active metals. The temporarily separated charge-discharge process of these active materials guarantees that Sn and the electrochemically active metals can operate as volume-releasing phases for each other alternately (Trifonova et al., 2002; Zhang, 2011). He and his co-workers have reported a colloidal synthesis of monodisperse SnSb nanocrystals that deliver high specific capacities of 700 and 600 mAh/g at 0.5 and 4.0°C after 100 cycles, respectively (He et al., 2015).

Graphene with its excellent electrical conductivity, flexibility, and high specific surface area can be an ideal buffering matrix for tin-based anodes (Li and Kaner, 2008). In 2015, Luo et al. synthesized a novel anode where tin nanoparticles were encapsulated into graphene backboned carbon foam (Luo B.

et al., 2016). Graphene and the outermost carbon coating serve as a physical boundary to prevent the aggregation of well-distributed tin nanoparticles and alleviate the huge volume changes of tin particles. The unique structure is prepared by uniformly growing  $\text{SnO}_2$  on the surface of graphene oxide and coating with porous carbon through a hydrothermal processes, finally calcinating in a reducing atmosphere. The resulting composite shows excellent cycle stability and exceptional rate performance in LIBs as well as in SIBs. A reversible specific capacity of 506 mAh  $\text{g}^{-1}$  can be achieved at a current density of 400 mAh/g and retained at 270 mAh/g, and even at 3,200 mA/g after 500 cycles (Figure 1). A summary of anode materials, synthetic methods, and electrochemical performance in tin-based anode composites is shown in Table 1 for comparison.

### SnO<sub>2</sub>-Based Composites

Tin oxide materials were first discovered and applied in LIBs with a high specific capacity by Idota et al. from Fuji Photo Film in 1997 (Idota et al., 1997). From then on,  $\text{SnO}_2$ -based anodes in LIBs have drawn considerable attention because of their high theoretical capacity, resource availability, environmental benignity, and low operating potentials (0.3 and 0.5 V vs.  $\text{Li}^+/\text{Li}$  in charge and discharge processes; Li R. et al., 2019). The chemical reactions of  $\text{SnO}_2$  with lithium electrodes involve the following two steps (Courtney and Dahn, 1997; Chen and Lou, 2013;

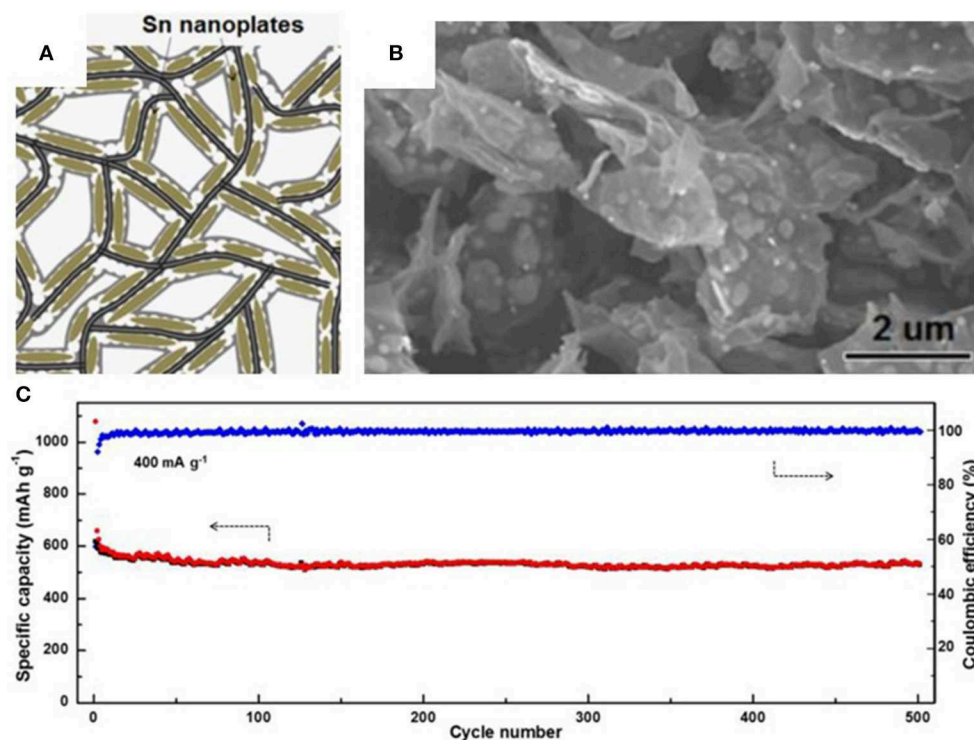


**FIGURE 1** | Schematic illustration (A) and SEM image (B) of tin nanoplates encapsulated in foam like graphene backboned carbonaceous carbon matrix (F-G/Sn@C), cycling performance (C) of F-G/Sn@C at 400 mA/g from 0.01 to 2.00 V. Reproduced from Luo B. et al. (2016) with permission from Copyright (2016) Elsevier.

**TABLE 1** | Anode materials, synthetic methods and electrochemical performance of a Sn-based anode.

Anode materials	Synthetic method	ICE (%)	Cyclability (mAh/g)	Rate performance (mAh/g)	References
Graphene/Sn@carbonaceous foam	Hydrothermal method and thermal reduction	About 60	777 (100 cycles at 100 mA/g)	506 (500 cycles at 400 mA/g) 270 (500 cycles at 3200 mA/g)	Luo B. et al., 2016
Sn@N-doped carbon	<i>In situ</i> polymerization and carbon thermal reduction	78.5	788 (300 cycles at 100 mA/g)	522 (1,000 cycles at 500 mA/g)	Chang et al., 2017
CoSn <sub>2</sub> /a-TiC/C	Ball milling	83.5	479 (180 cycles at 100 mA/g)	380 (500 mA/g)	Park et al., 2018
Core/shell Cu <sub>6</sub> Sn <sub>5</sub> @SnO <sub>2</sub> -C	Ball milling and heat treatment	65	619 (500 cycles at 200 mA/g)	390 (2 A/g)	Hu et al., 2015
Sn@hollow carbon cube	Combination of <i>in situ</i> chemical synthesis in aqueous solution, chemical vapor deposition (CVD) and acid etching	About 55	624 (200 cycles at 600 mA/g)	537 (1,000 cycles at 3 A/g)	Huang et al., 2015
C/Sn/C hollow spheres	<i>In situ</i> chemical synthesis in organic solution	62	1,100 (130 cycles at 100 mA/g)	430 (at 5 A/g)	Sun et al., 2019
Si@Sn-MoF	<i>In situ</i> chemical synthesis in organic solution	60.6	1,360 (250 cycles at 200 mA/g)	618 (800 cycles at 2 A/g)	Zhou et al., 2019
Sn@3D graphene networks	Freeze drying and chemical vapor deposition (CVD)	69	1,089 (100 at 200 mA/g)	459 (at 5 A/g) 270 (at 10 A/g)	Qin et al., 2014
Ni <sub>3</sub> Sn <sub>2</sub> microcages	Solvothermal reduction and crystallization	58.9	696 (400 cycles at 0.2 C) 530 (1,000 cycles at 1 C)	404 (at 10 C) 404 (at 10 C)	Liu J. et al., 2014
SnSb@N-doped carbon fiber	Electrospinning	72.2	892.6 (100 cycles at 100 mA/g)	487 (at 2 A/g)	Yuan et al., 2018

ICE, Initial coulombic efficiency.

Zhou et al., 2013b):



The theoretical specific capacity for bulk SnO<sub>2</sub> electrodes is 780 mAh/g, which includes conversion reactions and further alloying/dealloying reactions. It is worth noting that the conversion reactions of bulk SnO<sub>2</sub> to Sn are irreversible but can be partly reversible for nanosized SnO<sub>2</sub> and the theoretical specific capacity can be up to 1,484 mAh/g (Kim et al., 2005; Zhang et al., 2009). Like Sn, the as-formed Sn from SnO<sub>2</sub> suffers from huge volume changes (250%) in alloying/dealloying processes and what's worse, the inner stress originating from volume changes causes pulverization of the SnO<sub>2</sub> electrodes. The conversion reaction and pulverization of the SnO<sub>2</sub> electrode brings about a severe capacity decrease in the SnO<sub>2</sub>. Another issue that needs to be mentioned is that the Sn particles from conversion reactions tend to agglomerate into Sn clusters that will weaken the electrochemical activity (Park et al., 2007; Deng et al., 2016). These flaws are the main limitations for the commercialization of SnO<sub>2</sub>-based anodes in LIBs.

To deal with the defects of SnO<sub>2</sub>-based electrodes, the adopted strategies are summarized as follows. The first strategy is to convert bulk SnO<sub>2</sub> particles into nanosized particles and simultaneously design nanostructures such as nanospheres, nanotubes, and nanofilms (Liu et al., 2016). The nanostructures can accommodate volume changes and shorten the diffusion length for electrons and lithium ions, but the accompanying negative effect for nanostructure materials is that the high surface energy will lead to the agglomeration of nanoparticles, which is electrochemically unfavorable (Chen and Lou, 2013).

Additionally, structure design alone cannot compensate for the whole volume change whilst producing the desired electrochemical performance. Hence, another strategy is proposed, which is to combine the designed architecture with carbonaceous materials including carbon nanotubes, amorphous carbon, hard carbon, and graphene (Read et al., 2001; Yang et al., 2013; Zhou et al., 2016). Carbonaceous materials not only prevent nano SnO<sub>2</sub> and as-formed Sn grains from agglomeration by creating a physical barrier, but they also improve the overall electronic conductivity of the SnO<sub>2</sub>-based composite.

When it comes to size control of SnO<sub>2</sub> in LIBs, it is not found that as the SnO<sub>2</sub> particles get smaller, the better the electrochemical performance becomes. As the size of SnO<sub>2</sub> particles decreases, the SEI layer becomes larger, which hinders SnO<sub>2</sub> from reacting with lithium ions (Kim et al., 2013). According to Ahn et al., the optimum size of colloidal synthesis of SnO<sub>2</sub> particles is ~11 nm during Li<sup>+</sup> insertion/extraction processes (Ahn et al., 2004). A series of sizes of SnO<sub>2</sub> hollow spheres as investigated by Kim et al. demonstrated that SnO<sub>2</sub> hollow spheres with a size of 25 nm showed the best electrochemical performance (750 mAh/g after 50 cycles at a current density of 100 mA/g; Kim et al., 2013). Moreover, SnO<sub>2</sub> nanoparticles synthesized via the hydrothermal method with a size of 3 nm deliver the best reversible capacity (740 mAh/g after 60 cycles at 1,800 mA/g) compared to the ones at 4 and 8 nm (Kim et al., 2005). As a consequence, the optimum size for SnO<sub>2</sub> nanoparticles varies for different fabrication processes.

Recently, Jiang et al. have shown that well-designed cob-like SnO<sub>2</sub> nanoparticles coated with polydopamine and prepared by a hydrothermal processes exhibit an excellent rate capability and a long cycle life at around 1,400 mAh/g at a current density

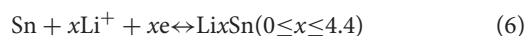
of 160 mA/g after 300 cycles (Jiang B. et al., 2017). Bush-like hydroxypropyl cellulose-graft-poly(acrylic acid) (HPC-g-PAA) and  $\text{Na}_2\text{SnO}_3 \cdot 3\text{H}_2\text{O}$  were used as the template and  $\text{SnO}_2$  precursor, respectively.  $\text{SnO}_2$  particles with an average size of 5 nm were uniformly grown on the graft of HPC-g-PAA template, and gaps of 3–5 nm among  $\text{SnO}_2$  particles could be observed, which allowed it to accommodate for volume changes of  $\text{SnO}_2$  particles in the electrode. Moreover, the final carbonized polydopamine coating was shown to help form stable SEI layers, which is helpful to enhance the cycle stability (Figure 2).

Beyond the use of carbon, transition metal compounds are also regarded as an effective component to be introduced into  $\text{SnO}_2$  electrodes with synergistic effects of combined materials.  $\text{TiO}_2$ , for example, is a very stable LIB anode material because of its outstanding electrochemical stability with only a slight volume change (3–4%) even in a high current density (Wang et al., 2012). However,  $\text{TiO}_2$  is restricted by a low theoretical capacity (178 mAh/g), so  $\text{TiO}_2$  is often used as a supporting backbone or a protective layer for unstable active materials like  $\text{SnO}_2$  (Liu H. et al., 2015). Tian et al. have proposed a well-designed nanostructure where  $\text{SnO}_2$  particles are encapsulated in  $\text{TiO}_2$  hollow nanowires (Tian et al., 2014). The composite employs  $\text{SnO}_2$  embedded carbon nanowires as a template after being coated with  $\text{TiO}_2$  and calcinated in air. Void spaces between  $\text{SnO}_2$  particles and  $\text{TiO}_2$  shells have been demonstrated through TEM analysis. The voids offer space to accommodate volume changes of  $\text{SnO}_2$  nanoparticles during the charge/discharge process. With this unique yolk-shell structure and the role of  $\text{TiO}_2$  in the composite, the final  $\text{SnO}_2@/\text{TiO}_2$  composite exhibits a great cycle stability (445 mAh/g at a current density of 800 mA/g after 500 cycles). A summary of anode materials, synthetic methods, and electrochemical performances upon some  $\text{SnO}_2$ -based anodes are pointed out in Table 2.

## SnS<sub>2</sub>-Based Composites

Momma et al. and Brousse et al. have revealed that tin sulfides could also be used as novel anode materials in

LIBs (Brousse et al., 1998; Momma et al., 2001).  $\text{SnS}_2$  materials possess superior physicochemical properties with a theoretical specific capacity of 645 mAh/g and a unique layered hexagonal CdI<sub>2</sub>-type crystal structure that is composed of tin cations sandwiched between two layers of close-packed sulfur anions in octahedral coordination, in which adjacent sulfur layers are linked with weak Van der Waals interactions and the interlayer intervals are about 0.59 nm (Morales et al., 1992; Lefebvre et al., 1997; Song et al., 2013; Deng et al., 2014; Li R. et al., 2019). Layer voids in this unique configuration are beneficial for the  $\text{Li}^+$  insertion process and can partially accommodate the volume change (Chen et al., 2017). However, integral volume changes and poor electronic conductivity of  $\text{SnS}_2$  are inevitable, which needs to be improved and one set of adopted electrochemical reactions have been put forward, which are the following (Momma et al., 2001; Kim et al., 2007):



It can be obviously observed from the above equations that the reaction mechanism of  $\text{SnS}_2$  with lithium is very similar to the lithiation and delithiation of  $\text{SnO}_2$ . In the first discharge cycle, metallic tin and amorphous  $\text{Li}_2\text{S}$  are formed during the irreversible conversion of  $\text{SnS}_2$ , where active Sn can be coated with the inactive  $\text{Li}_2\text{S}$ , mitigating the volume changes of the electrode to some extent (Kim et al., 2009). With further charge and discharge processes, alloying/dealloying reactions of tin with lithium ions are reversible, but the capacity reduces rapidly due to the irreversible conversion and severe pulverization of  $\text{SnS}_2$  electrodes. Analogously, morphology design and the introduction of a conductive phase that accommodates volume changes, like amorphous carbon and graphene, can largely alleviate the volume changes of  $\text{SnS}_2$  in charge and discharge processes (Zhuo et al., 2012).

Since the microstructure of layered  $\text{SnS}_2$  materials has some resemblance to 2D graphene, the combination of them is more

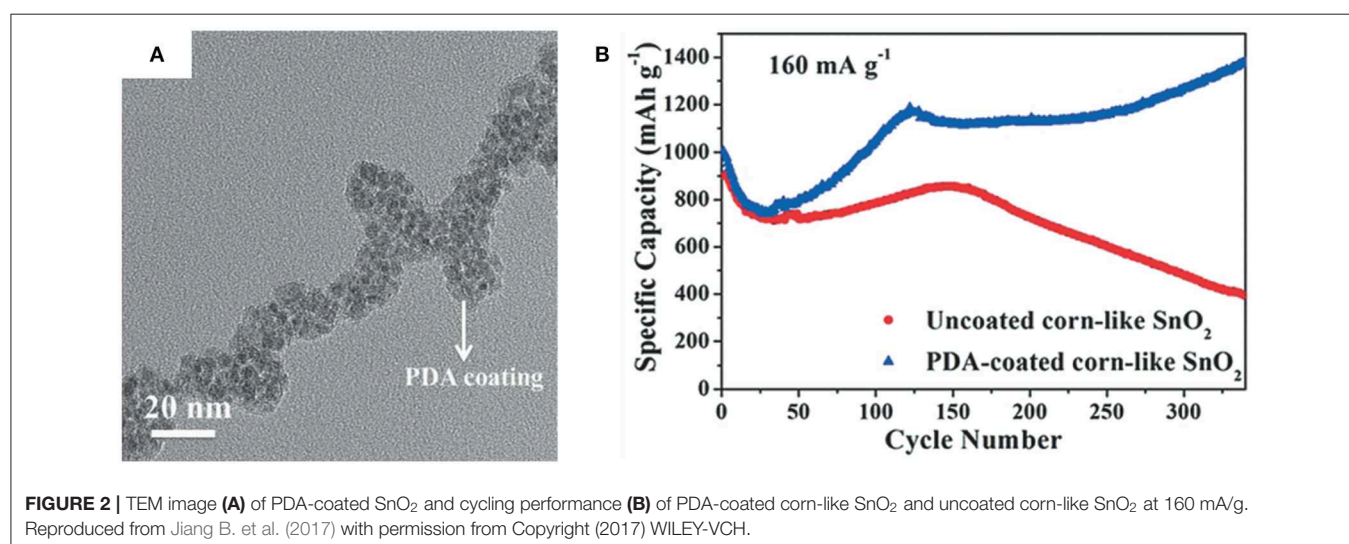


**TABLE 2** | Anode materials, synthetic methods and electrochemical performance of SnO<sub>2</sub>-based composites in LIBs.

Anode materials	Synthetic method	ICE (%)	Cyclability (mAh/g)	Rate performance (mAh/g)	References
Corn-like SnO <sub>2</sub> nanocrystals/polydopamine	Combination of atom transfer radical polymerization, hydrothermal method and thermal treatment	61.3	1,494 (300 cycles at 160 mA/g)	835 (at 1A/g) 667 (at 2A/g)	Jiang B. et al., 2017
SnO <sub>2</sub> @TiO <sub>2</sub>	Hydrothermal synthesis and heat treatment	46.8	445 (500 cycles at 800 mA/g)	222 (at 1.6 A/g) 204 (at 2.0 A/g)	Tian et al., 2014
sSnO <sub>2</sub> @N-doped graphene	Hydrothermal treatment and thermal reduction	61.3	1,346 (500 cycles at 100 mA/g from)	631 (at 10 A/g)	Zhou et al., 2013b
SnO <sub>2</sub> quantum dots/graphene oxide	Hydrothermal synthesis	about 53	112 (100 cycles at 100 mA/g)	417 (2,000 cycles at 2 A/g)	Zhao et al., 2016
F-doped SnO <sub>2</sub> @reduced graphene oxide (rGO)	Hydrothermal synthesis	60.5	1,037 (150 cycles at 100 mA/g)	860 (at 1 A/g) 770 (at 2 A/g)	Cui, 2017
Microwave-assisted SnO <sub>2</sub> @polypyrrole nanotube	Soft-template polymerization and microwave-assisted solvothermal synthesis	58.1	790 (200 cycles at 200 mA/g)	860 (at 1 A/g) 770 (at 2 A/g)	Du et al., 2016
SnO <sub>2</sub> @N-doped carbon fiber	Electrospinning and heat treatment	69.2	754 (300 cycles at 1,000 mA/g)	527 (at 1.6 A/g) 405 (at 3.2 A/g)	Xia et al., 2016

ICE, Initial coulombic efficiency.

compatible than other dissimilar materials like SnO<sub>2</sub>, Sn, and Si (Bin et al., 2019). Few-layer SnS<sub>2</sub>/graphene hybrid materials synthesized using L-cysteine as a ligand in the solution-phase method have been reported by Chang et al. which can deliver a reversible specific capacity of 920 mAh/g at a current density of 100 mA/g (Chang et al., 2012). Additionally, graphene can be functionalized by doping with nitrogen, fluorine, or sulfur elements, and the doped graphene generates more defects and active sites which significantly enhances the electrochemical activity and conductivity (Guo et al., 2011). Zheng et al. have reported a large-scale and facile synthetic route for SnS<sub>2</sub> nanoparticles coated with S-doped graphene (SnS<sub>2</sub>/S-rGO). The electrochemical stability of SnS<sub>2</sub>/S-rGO particles is much better than that of the undoped SnS<sub>2</sub>/rGO, in which the SnS<sub>2</sub>/S-rGO can possess a discharge specific capacity of 947 mAh/g whereas the SnS<sub>2</sub>/rGO is about 700 mAh/g after 200 cycles at 1A/g (Zheng et al., 2017). This result can be mainly ascribed to the stronger interaction of S-doped graphene with SnS<sub>2</sub> particles.

Wu et al. have presented a well-designed stable H-TiO<sub>2</sub>@SnS<sub>2</sub>@PPy composite by growing SnS<sub>2</sub> sheets on hydrogen treated TiO<sub>2</sub> (H-TiO<sub>2</sub>) nanowires and coating with carbonized polypyrrole (PPy), in which H-TiO<sub>2</sub> provides some advantages over untreated TiO<sub>2</sub>. The key reason is that H-TiO<sub>2</sub> structurally possesses more defects than the untreated TiO<sub>2</sub>, which provides increased conductivity and stronger chemical interactions with SnS<sub>2</sub> (Ti-S) (Wu et al., 2019). Furthermore, the outermost carbonized PPy layer can accommodate the volume change to some degree as well as boosting the electronic conductivity. With the synergistic effects of the mentioned materials, the final H-TiO<sub>2</sub>@SnS<sub>2</sub>@PPy composite can deliver an outstanding electrochemical stability with a high discharge specific capacity of 508.7 mAh/g at 2.0 A/g after 2,000 cycles (Figure 3). A summary of anode materials, synthetic methods, and electrochemical performance of SnS<sub>2</sub>-based composites in LIBs have been displayed in Table 3.

## TIN AND TIN COMPOUNDS IN SIBs

The revival of sodium-ion batteries (SIBs) owes mainly to the low cost and abundance of sodium on earth. Although the intercalation mechanism of sodium and lithium are similar when used as electrodes in secondary alkali metal batteries, the larger radius size of Na<sup>+</sup> (1.09 Å) compared to Li<sup>+</sup> (0.74 Å) makes it challenging to find a suitable Na<sup>+</sup> host with both excellent cycle stability and a relatively high capacity (Luo W. et al., 2016; Wu L. et al., 2018). Graphite is the most used anode in commercial LIBs but cannot insert Na<sup>+</sup> effectively, which is due to the mismatching of graphite's interlayer interval (0.334 nm) with the larger radius of Na<sup>+</sup> (Chevrier and Ceder, 2011). Moreover, Si is a very promising anode material for LIBs as it has a theoretical discharge specific capacity of 3,579 mAh/g, and some Si-based materials have been commercialized, but it cannot react with Na<sup>+</sup> in the same manner as LIBs. This is because Na-induced lattice disturbance are remarkable in Si materials as they become endowed with small interstitial space and high stiffness (Chou et al., 2015; Fang et al., 2019). Interestingly, Sn, SnO<sub>2</sub>, and SnS<sub>2</sub> can be applied in SIBs with relatively high capacity, low cost, and proper low charge/discharge potentials vs. Na/Na<sup>+</sup>, due to the minor Na-induced lattice disturbance in Sn-based materials (Guo et al., 2011; Zhu et al., 2013; Li et al., 2015). However, these active materials still go through huge volume changes, and the volume change is even severer in SIBs, which leads to serious pulverization of these brittle active materials ending up with rapid capacity decay and poor cycle stability (Ellis et al., 2012). The coping strategies of Sn, SnO<sub>2</sub>, and SnS<sub>2</sub> in SIBs are analogous to ones in LIBs, which are the nanostructure design of these active materials and the process of simultaneously introducing a second phase that buffers the volume change (Nayak et al., 2018). Major improvements for Sn, SnO<sub>2</sub>, and SnS<sub>2</sub> in SIBs have been separately detailed in the following sections and the anode materials, synthetic methods and electrochemical performance of

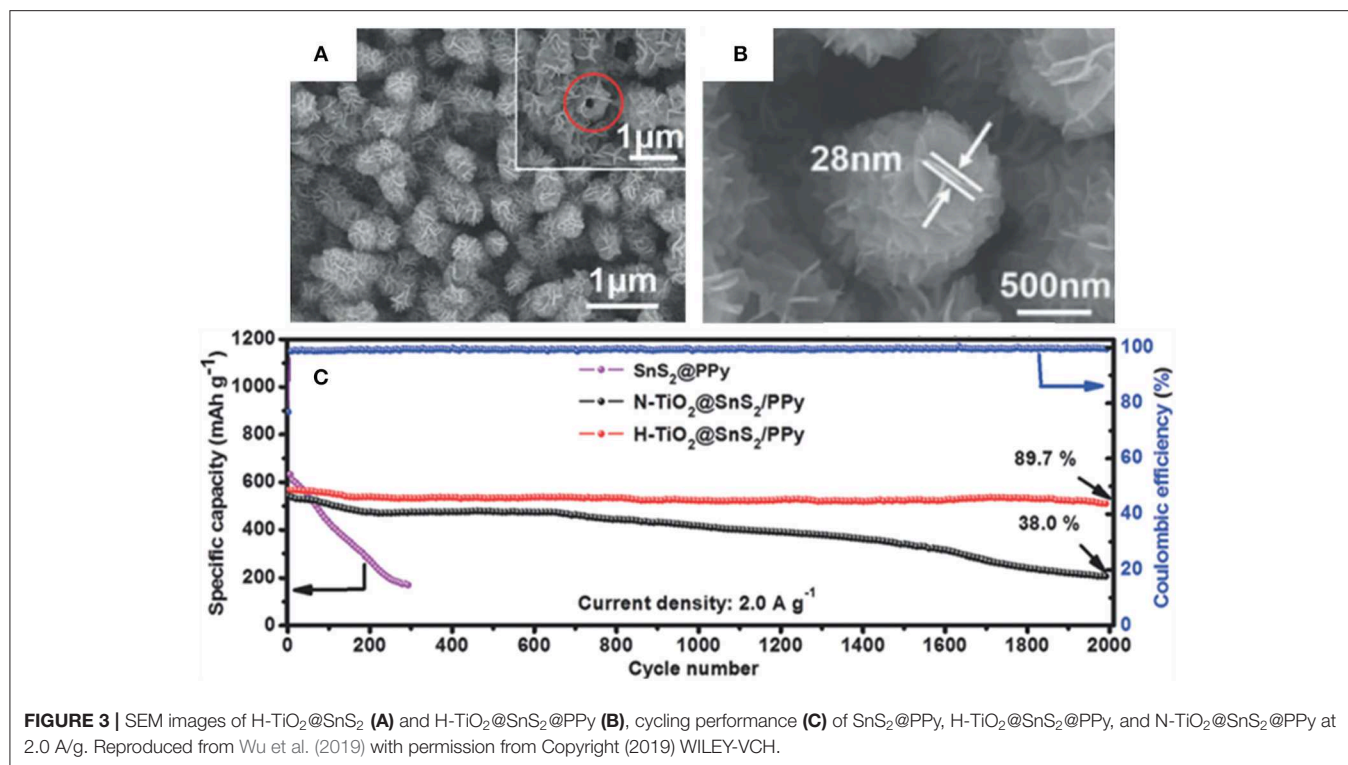


**TABLE 3** | Anode materials, synthetic methods and electrochemical performance of SnS<sub>2</sub>-based composites in LIBs.

Anode materials	Synthetic method	ICE (%)	Cyclability (mAh/g)	Rate performance (mAh/g)	References
H-TiO <sub>2</sub> @SnS <sub>2</sub> @PPy	Combination of hydrolysis, hydrothermal route, thermal treatment and polymerization	71.2	508.7 (2,000 cycles at 2 A/g)	356.3 (at 10 A/g)	Wu et al., 2019
Few-layer SnS <sub>2</sub> /graphene	Hydrothermal method	42.4	920 (50 cycles at 100 mA/g)	520 (at 1 A/g)	Chang et al., 2012
SnS <sub>2</sub> /Sulfur doped graphene	Wet chemistry method	72	947 (200 cycles at 1 A/g)	550 (at 5 A/g)	Zheng et al., 2017
Porous vanadium nitride (VN)@SnS <sub>2</sub>	Hydrothermal method	77	819 (100 cycles at 650 mA/g)	349 (at 13 A/g)	Balogun et al., 2015
MoS <sub>2</sub> /SnS <sub>2</sub> -graphene oxide (GO)	One-pot hydrothermal synthesis	84.2	1,244 (190 cycles at 150 mA/g)	456 (at 3.8 A/g)	Jiang Y. et al., 2017
SnS <sub>2</sub> @PANI nanoplates	Hydrothermal and polymerization process	69.4	730.8 (80 cycles at 100 mA/g)	559.2 (at 2 A/g) 356.1 (at 5 A/g)	Wang G. et al., 2015
SnS <sub>2</sub> /graphene/ SnS <sub>2</sub>	Hydrothermal synthesis	81	1,357 (200 cycles at 100 mA/g)	844 (at 10 A/g)	Jiang et al., 2019

ICE, Initial coulombic efficiency.

Sn, SnO<sub>2</sub>, SnS<sub>2</sub>-based anode composites in SIBs are summarized in **Table 4**.

## Sn-Based Composites

The theoretical capacity of Sn as anode materials in SIBs (Na<sub>15</sub>Sn<sub>4</sub>) is about 847 mAh/g, but volume changes of Sn electrodes during charge-discharge processes are as high as 525 %, which is much higher than Sn in LIBs (Qian et al., 2014). As reported by Qian et al., the capacity of pure Sn electrodes in SIBs falls to zero in only five cycles, which can be explained by the pulverization of active materials during Na<sup>+</sup> insertion/extraction processes (Ellis et al., 2013). Sn-based intermetallic alloy anodes

have been demonstrated to be a reasonable solution to address the short cycle life of Sn (Li J. et al., 2019). A Sn-Cu alloy is a stable active/inactive alloy with a relatively high capacity in LIBs where the addition of Cu significantly increases the stability of the alloy. As mentioned in the LIBs section, the Cu<sub>6</sub>Sn<sub>5</sub> alloy is more stable than other Sn-Cu intermetallics, but the application of Cu<sub>6</sub>Sn<sub>5</sub> in SIBs is hampered by the short diffusion depth owing to the larger size of Na<sup>+</sup>. Regarding this, Lin et al. have reported using a Sn<sub>0.9</sub>Cu<sub>0.1</sub> alloy in SIBs (Lin et al., 2013). In spite of a low initial discharge specific capacity of 250 mAh/g, the capacity gradually increased to 440 mAh/g in 20 cycles without capacity loss after 100 cycles.

**TABLE 4** | Anode materials, synthetic methods and electrochemical performance of Sn, SnO<sub>2</sub>, and SnS<sub>2</sub>-based composite anodes in SIBs.

Anode materials	Synthetic method	ICE (%)	Cyclability (mAh/g)	Rate performance (mAh/g)	References
Sn <sub>0.9</sub> Cu <sub>0.1</sub>	Surfactant-assistant wet chemistry	—	420 (100 cycles at 169 mA/g)	126 (at 1.694 A/g)	Lin et al., 2013
Yolk-shell Sn <sub>4</sub> P <sub>3</sub> @C	Hydrothermal treatment and thermal reduction	43.8	515 (50 cycles at 100 mA/g)	421 (at 3 A/g)	Liu J. et al., 2015
SnSb/C composite	Mechanical milling	75.1	435 (50 cycles at 100 mA/g)	274 (at 1 A/g)	Xiao et al., 2012
Porous Ni <sub>3</sub> Sn <sub>2</sub> microcages	Solvothermal reduction and crystallization	35.5	270 (300 cycles at 1A/g)	351 (at 5 A/g) 276 (at 10 A/g)	Liu J. et al., 2014
C@SnS/SnO <sub>2</sub> @graphene	Hydrothermal synthesis and sulfidation	74.6	713 (70 cycles at 30 mA/g)	550 (at 810 mA/g) 430 (at 2430 mA/g)	Zheng et al., 2016
MoS <sub>2</sub> @SnO <sub>2</sub> @C	Hydrothermal method and thermal treatment	67.99	396 (150 cycles at 50 mA/g)	168 (at 2 A/g)	Chen et al., 2018
SnO <sub>2</sub> @graphene	Hydrothermal synthesis	About 30.9	638 (100 cycles at 20 mA/g)	263 (320 mA/g) 143 (640 mA/g)	Su et al., 2013
Porous SnO <sub>2</sub> /Cu foil	Cold rolling method and anodization	73	326 (200 cycles at 200 mA/g)	232 (at 2 A/g) 150 (at 5 A/g)	Bian et al., 2016
Exfoliated SnS <sub>2</sub> /graphene	Sol-gel method and hydrothermal treatment	69	618.9 (100 cycles at 200 mA/g)	326 (at 4 A/g)	Liu Y. et al., 2014
SnS <sub>2</sub> /C nanospheres	Solid-state fabrication	about 54.5	600 (100 cycles at 50 mA/g)	360 (at 1 A/g)	Wang J. et al., 2015
SnS <sub>2</sub> /graphene/SnS <sub>2</sub>	Hydrothermal synthesis	66.8	1133 (100 cycles at 100 mA/g)	765 (at 10 A/g)	Jiang et al., 2019
TiO <sub>2</sub> @SnS <sub>2</sub> @Nitrogen-doped carbon	Combination of chemical synthesis in organic solution, hydrothermal synthesis and ALD	64.2	293 (600 cycles at 1 A/g)	152 (at 10 A/g)	Ren et al., 2018
Graphene/Sn@carbonaceous foam	Hydrothermal method and thermal reduction	About 55.1	434.2 (100 cycles at 100 mA/g)	166 (at 1.6 A/g) 3.2 (at 3.2 A/g)	Luo B. et al., 2016
MoS <sub>2</sub> /SnS <sub>2</sub> -graphene oxide (GO)	One-pot hydrothermal synthesis	76.5	655 (100 cycles at 150 mA/g)	550 (at 1.5 A/g) 340 (at 6.0 A/g)	Jiang Y. et al., 2017

ICE, Initial coulombic efficiency.

Sn-P intermetal is an emerging SIB anode material with balanced properties (Luo W. et al., 2016). Although the theoretical specific capacity of Sn<sub>4</sub>P<sub>3</sub> (1,132 mAh/g) is significantly inferior to the pure P (2,560 mAh/g), electronic conductivity and theoretical volumetric capacity are much better than pure P in SIBs (Kim et al., 2014; Lan et al., 2017). Liu et al. have synthesized uniform yolk-shell Sn<sub>4</sub>P<sub>3</sub>@C nanoparticles for SIBs where Sn<sub>4</sub>P<sub>3</sub> nanoparticles are encapsulated in hollow carbon spheres rendering some void space for the volume change of Sn<sub>4</sub>P<sub>3</sub> whilst maintaining an intact microstructure (Liu J. et al., 2015). The carbon shell helps to form a stable SEI layer and strengthen the overall electronic conductivity of the composite. An initial discharge specific capacity of 790 mAh/g for yolk-shell Sn<sub>4</sub>P<sub>3</sub>@C nanospheres was determined and retained a high reversible specific capacity of 515 mAh/g after 50 cycles at 100 mA/g (Figure 4).

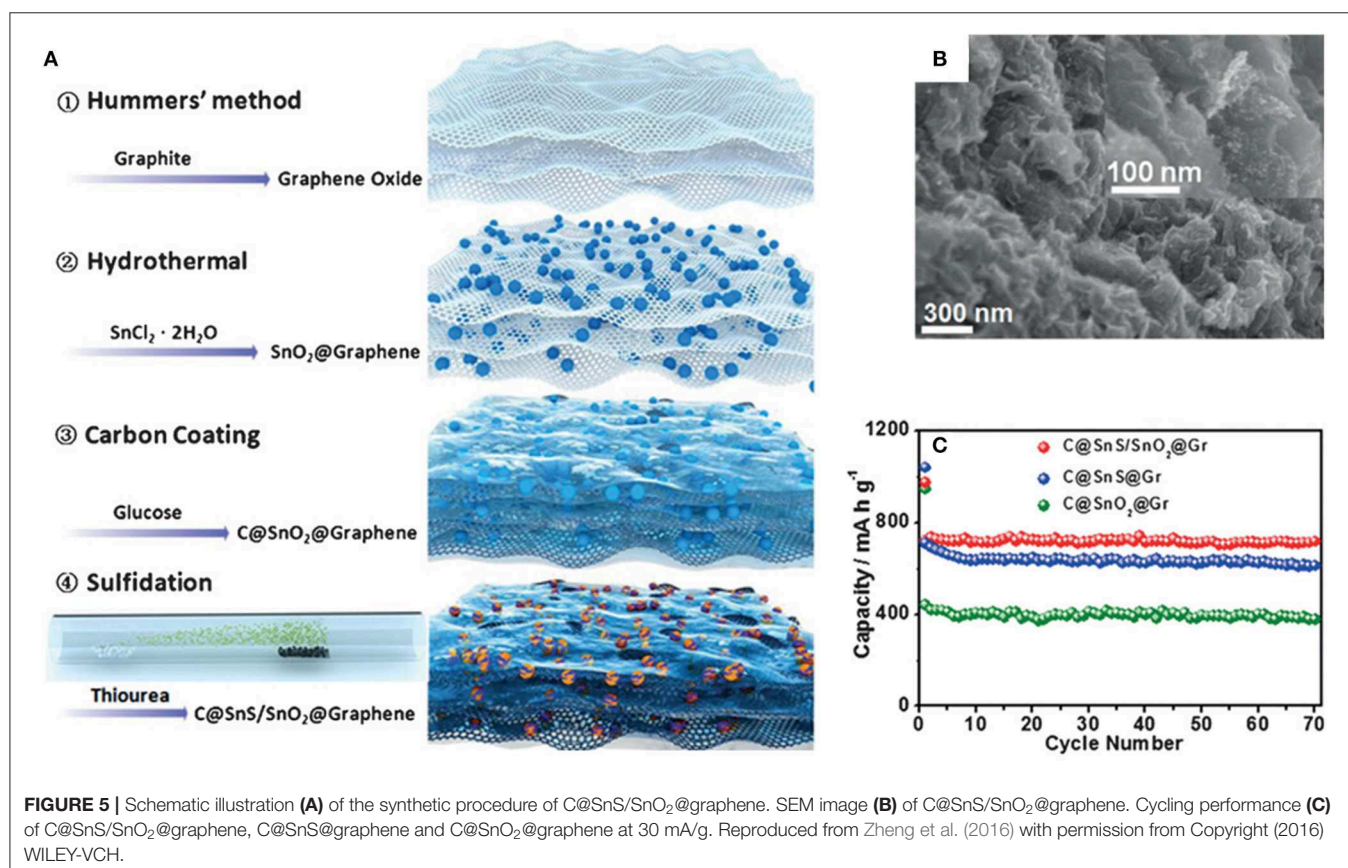
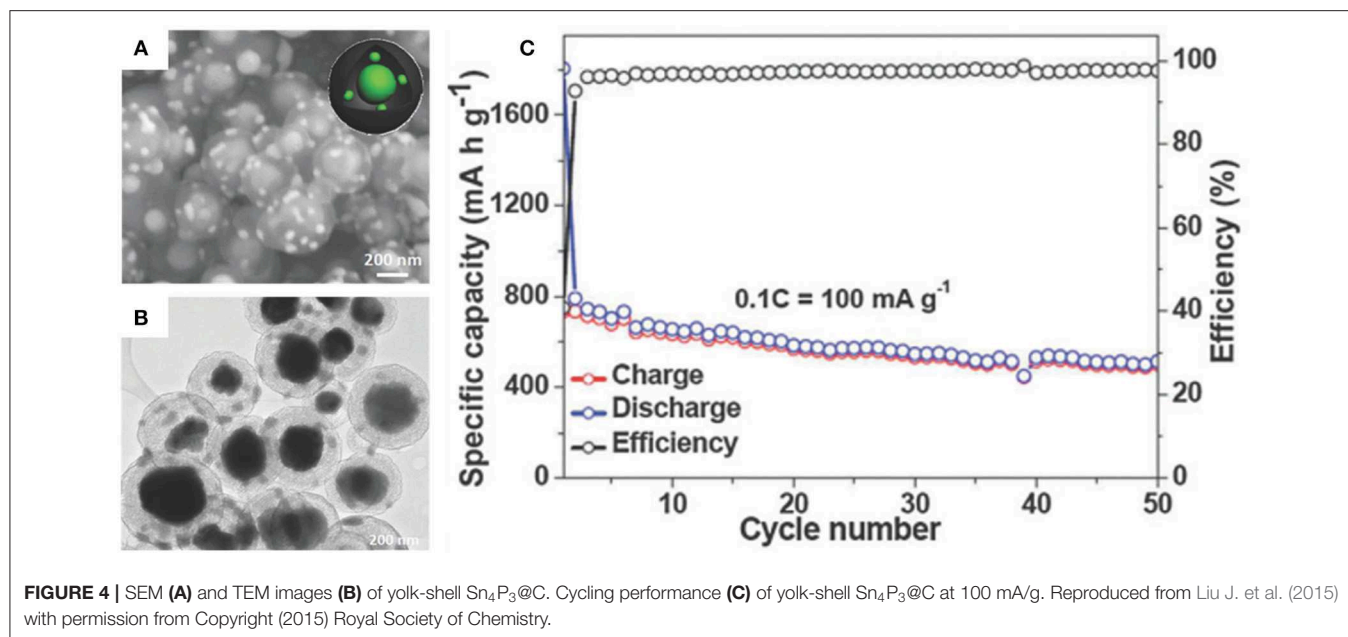
## SnO<sub>2</sub>-Based Composites

Sodiation/desodiation reactions of the SnO<sub>2</sub> electrode are very similar to the lithiation/delithiation process, which include the conversion of SnO<sub>2</sub> and reversible alloying/dealloying reactions contributing to the total theoretical specific capacity of 1,378 mAh/g (Su et al., 2013). SnO<sub>2</sub> is one of the most extensively investigated anode materials in LIBs and nowadays, some of the SnO<sub>2</sub>-based composites have reached the theoretical capacity of SnO<sub>2</sub> with an excellent cycle life.

Herein, successful strategies in LIBs to address volume changes are advised for employment in SIBs as well (Chen and Lou, 2013).

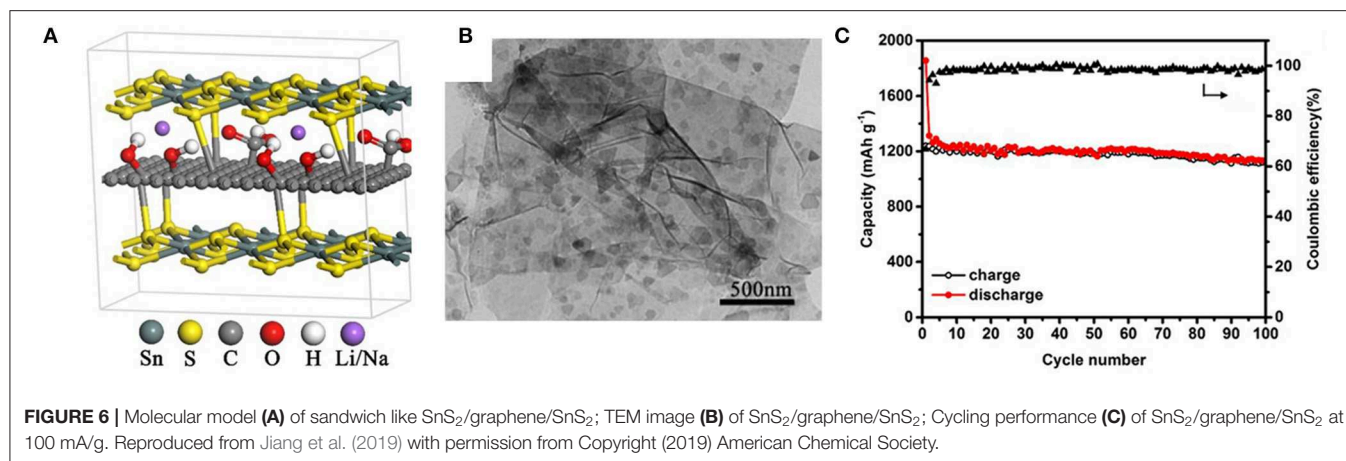
Huang et al. have reported a facile *in situ* synthesis of 3D porous carbon encapsulated SnO<sub>2</sub> nanoparticles (SnO<sub>2</sub>-PC) that exhibits a great cycle stability with a discharge specific capacity of 208.1 mAh/g at 100 mA/g after 250 cycles and SnO<sub>2</sub>-PC with a SnO<sub>2</sub> weight percentage of 74.47 % demonstrated an extraordinary rate capability with a discharge specific capacity of 100 mAh/g at 1,600 mA/g after 1,000 cycles (Huang et al., 2016). The greatly improved electrochemical performance of the as-prepared SnO<sub>2</sub>-PC composite owes to the porous carbon matrix that can alleviate volume changes of SnO<sub>2</sub> in the sodiation/desodiation process and improve the electronic conductivity of the composite.

Heterostructure has the advantage of high-speed electron transfer because of the interface effect. The heterojunction of nanocrystals with different band-gaps has been proven to enhance surface reaction kinetics and to provide increased charge transport. Zheng et al. have employed SnS in a C@SnO<sub>2</sub>@graphene composite in SIBs. The C@SnS/SnO<sub>2</sub>@graphene composite exhibits a high rate capability and long cycle life with a high capacity, which can be ascribed to the heterostructure of SnS/SnO<sub>2</sub> which further improves the electronic conductivity and



diffusion of  $\text{Na}^+$  in the electrode (Zheng et al., 2016).  $\text{C}@\text{SnS}/\text{SnO}_2@\text{graphene}$  achieves a reversible discharge specific capacity of 713 mAh/g at 30 mA/g after 70 cycles, which is higher than  $\text{C}@\text{SnS}@\text{graphene}$  (around 600 mAh/g) and

$\text{C}@\text{SnO}_2@\text{graphene}$  (around 400 mAh/g). By increasing the current density to 810 and 2,430 mA/g, the discharge specific capacity can be retained at 520 and 430 mAh/g, respectively (Figure 5).



## SnS<sub>2</sub>-Based Composites in SIBs

As mentioned, SnS<sub>2</sub> has a special layered structure where tin cations are sandwiched between two layers of sulfur anions. The spacing between two adjoining two layers ( $d_{002} = 5.90 \text{ \AA}$ ) is larger than the radius of Na<sup>+</sup> ( $d_{002} = 1.09 \text{ \AA}$ ), which allows the intercalation and diffusion of Na<sup>+</sup> throughout the electrode effectively (Zheng et al., 2016). However, a pure SnS<sub>2</sub> electrode contends with poor conductivity and severe pulverization. It has been demonstrated from previous studies that combining SnS<sub>2</sub> with conductive materials will notably strengthen the electrochemical performance (Ren et al., 2017; Wu Y. et al., 2018). The unique 2D layer structure of SnS<sub>2</sub> means it is highly compatible with graphene and can provide an increase in electronic conductivity. In 2014, Liu et al. discovered that exfoliated SnS<sub>2</sub> restacked on graphene showed a remarkable electrochemical performance with a discharge specific capacity of 650 mAh/g at 200 mA/g after 100 cycles (Liu Y. et al., 2014). The excellent performance can be ascribed to the ultrasmall exfoliated-SnS<sub>2</sub> layers being utilized fully when used as the electrode.

Jiang et al. have reported a sandwich-like SnS<sub>2</sub>/graphene/SnS<sub>2</sub> composite with expanded interlayers produced by a one-step hydrothermal synthesis, where both sides of the reduced graphene oxide sheets is covalently decorated with ultrathin SnS<sub>2</sub> nanosheets (Jiang et al., 2019). The enlarged interlayer distance of SnS<sub>2</sub> is about 8.03 Å, which assists the insertion/extraction of Li<sup>+</sup>/Na<sup>+</sup> with rapid transport kinetics. As a result, SnS<sub>2</sub>/graphene/SnS<sub>2</sub> composites have excellent electrochemical properties both in LIBs (see also in the LIBs section) and SIBs. To be specific for SIBs, the reversible discharge specific capacities of 1,295 mAh/g and 765 mAh/g are delivered at a current density of 0.1 and 10 A/g, respectively (Figure 6). Additionally, according to the structural characterizations of SnS<sub>2</sub>/graphene/SnS<sub>2</sub> electrodes after 200 cycles, morphology changes and significant particle agglomeration cannot be clearly detected. Some reasons for the superiority of the SnS<sub>2</sub>/graphene/SnS<sub>2</sub> composite are that the graphene sheet is sandwiched between

SnS<sub>2</sub> layers with enhanced conductivity and it has a strong structural integrity.

## SUMMARY AND OUTLOOK

Sn, SnO<sub>2</sub>, and SnS<sub>2</sub> have been extensively studied as substitutes for graphite in LIBs and for potential application in SIBs. Either in LIBs or SIBs, the ultimate problem that needs to be addressed is the huge volume change of Sn with Li<sup>+</sup> or Na<sup>+</sup> during the alloying/dealloying processes. This problem has been largely addressed by introducing one or more metals and/or compounds into the system and at least one additive which can act as an inactive buffering matrix. Also, the use of reasonable nanostructure design can tactfully mitigate the volume change and facilitate the diffusion of Li<sup>+</sup> (Na<sup>+</sup>) and electrons. Due to these efforts, some of these tin-based anode materials have reached their maximum theoretical capacity. So far, the real practical uses of tin-based anodes is still very scarce in both LIBs and SIBs, which is mainly due to the tedious synthetic procedures, high costs and low yields. Recently, much work has focused on large-scale synthetic methods. We believe that a cost-effective and facile fabrication process which takes morphology into consideration can promote the application of tin-based anodes in commercial LIBs and large-scale energy storage equipment in SIBs.

## AUTHOR CONTRIBUTIONS

HM and WX contributed conception and design of the study. CM, RL, and LY organized the database. HM wrote the first draft of the manuscript. WX revised the whole manuscript.

## FUNDING

This work was financially supported by the National Natural Science Foundation of China (Nos. 51874046 and 51404038).

## REFERENCES

- Ahn, H.-J., Choi, H.-C., Park, K.-W., Kim, S.-B., and Sung, Y.-E. (2004). Investigation of the structural and electrochemical properties of size-controlled SnO<sub>2</sub> nanoparticles. *J. Phys. Chem. B* 108, 9815–9820. doi: 10.1021/jp035769n
- Balogun, M.-S., Qiu, W., Jian, J., Huang, Y., Luo, Y., Yang, H., et al. (2015). Vanadium nitride nanowire supported SnS<sub>2</sub> nanosheets with high reversible capacity as anode material for lithium ion batteries. *ACS Appl. Mater. Inter.* 7, 23205–23215. doi: 10.1021/acsami.5b07044
- Beaulieu, L. Y., Eberman, K. W., Turner, R. L., Krause, L. J., and Dahn, J. R. (2001). Colossal reversible volume changes in lithium alloys. *Electrochem. Solid-State Lett.* 4, A137–A140. doi: 10.1149/1.1388178
- Bian, H., Zhang, J., Yuen, M.-F., Kang, W., Zhan, Y., Yu, D. Y. W., et al. (2016). Anodic nanoporous SnO<sub>2</sub> grown on Cu foils as superior binder-free Na-ion battery anodes. *J. Power Sources* 307, 634–640. doi: 10.1016/j.jpowsour.2015.12.118
- Bin, D.-S., Duan, S.-Y., Lin, X.-J., Liu, L., Liu, Y., Xu, Y.-S., et al. (2019). Structural engineering of SnS<sub>2</sub>/graphene nanocomposite for high-performance K-ion battery anode. *Nano Energy* 60, 912–918. doi: 10.1016/j.nanoen.2019.04.032
- Brousse, T., Lee, S. M., Pasquereau, L., Defives, D., and Schleich, D. M. (1998). Composite negative electrodes for lithium ion cells. *Solid State Ion.* 113–115, 51–56. doi: 10.1016/S0167-2738(98)00366-X
- Chang, K., Wang, Z., Huang, G., Li, H., Chen, W., and Lee, J. Y. (2012). Few-layer SnS<sub>2</sub>/graphene hybrid with exceptional electrochemical performance as lithium-ion battery anode. *J. Power Sources* 201, 259–266. doi: 10.1016/j.jpowsour.2011.10.132
- Chang, X., Wang, T., Liu, Z., Zheng, X., Zheng, J., and Li, X. (2017). Ultrafine Sn nanocrystals in a hierarchically porous N-doped carbon for lithium ion batteries. *Nano Res.* 10, 1950–1958. doi: 10.1007/s12274-016-1381-6
- Chen, J. S., and Lou, X. W. (2013). SnO<sub>2</sub>-based nanomaterials: synthesis and application in lithium-ion batteries. *Small* 9, 1877–1893. doi: 10.1002/smll.201202601
- Chen, Q., Lu, F., Xia, Y., Wang, H., and Kuang, X. (2017). Interlayer expansion of few-layered Mo-doped SnS<sub>2</sub> nanosheets grown on carbon cloth with excellent lithium storage performance for lithium ion batteries. *J. Mater. Chem. A* 5, 4075–4083. doi: 10.1039/C7TA00236J
- Chen, Z., Yin, D., and Zhang, M. (2018). Sandwich-like MoS<sub>2</sub>@SnO<sub>2</sub>@C with high capacity and stability for sodium/potassium ion batteries. *Small* 14, 1703818. doi: 10.1002/smll.201870074
- Chevrier, V. L., and Ceder, G. (2011). Challenges for Na-ion negative electrodes. *J. Electrochem. Soc.* 158, A1011–A1014. doi: 10.1149/1.3607983
- Chou, C.-Y., Lee, M., and Hwang, G. S. (2015). A comparative first-principles study on sodiation of silicon, germanium, and tin for sodium-ion batteries. *J. Phys. Chem. C* 119, 14843–14850. doi: 10.1021/acs.jpcc.5b01099
- Courtney, I. A., and Dahn, J. R. (1997). Electrochemical and in situ X-ray diffraction studies of the reaction of lithium with tin oxide composites. *J. Electrochem. Soc.* 144, 2045–2052. doi: 10.1149/1.1837740
- Cui, D. (2017). Fluorine-doped SnO<sub>2</sub> nanoparticles anchored on reduced graphene oxide as a high-performance lithium ion battery anode. *J. Power Sources* 362:20–26. doi: 10.1016/j.jpowsour.2017.07.024
- Dahn, J. R., Mar, R. E., and Abouzeid, A. (2006). Combinatorial study of Sn<sub>1-x</sub>Co<sub>x</sub> (0 < x < 0.6) and [Sn<sub>0.55</sub>Co<sub>0.45</sub>]<sub>1-y</sub>C<sub>y</sub> (0 < y < 0.5) alloy negative electrode materials for Li-ion batteries. *J. Electrochem. Soc.* 153, A361–A365. doi: 10.1149/1.2150160
- Dang, H. X., Klavetter, K. C., Meyerson, M. L., Heller, A., and Mullins, C. B. (2015). Tin microparticles for a lithium ion battery anode with enhanced cycling stability and efficiency derived from Se-doping. *J. Mater. Chem. A* 3, 13500–13506. doi: 10.1039/C5TA02131F
- Deng, Y., Fang, C., and Chen, G. (2016). The developments of SnO<sub>2</sub>/graphene nanocomposites as anode materials for high performance lithium ion batteries: a review. *J. Power Sources* 304, 81–101. doi: 10.1016/j.jpowsour.2015.11.017
- Deng, Y., Luo, Z., Conrad, N. J., Liu, H., Gong, Y., Najmaei, S., et al. (2014). Black phosphorus-monolayer MoS<sub>2</sub> van der Waals heterojunction p-n diode. *ACS Nano* 8, 8292–8299. doi: 10.1021/nn5027388
- Du, X., Yang, T., Lin, J., Feng, T., Zhu, J., Lu, L., et al. (2016). Microwave-assisted synthesis of SnO<sub>2</sub>@polypyrrole nanotubes and their pyrolyzed composite as anode for lithium-ion batteries. *ACS Appl. Mater. Interfaces.* 8, 15598–15606. doi: 10.1021/acsami.6b03332
- Ellis, L. D., Ferguson, P. P., and Obrovac, M. N. (2013). Sodium insertion into tin cobalt carbon active/inactive nanocomposite. *J. Electrochem. Soc.* 160, A869–A872. doi: 10.1149/2.103306jes
- Ellis, L. D., Hatchard, T. D., and Obrovac, M. N. (2012). Reversible insertion of sodium in tin. *J. Electrochem. Soc.* 159, A1801–A1805. doi: 10.1149/2.037211jes
- Fang, R., Miao, C., Mou, H., and Xiao, W. (2020). Facile synthesis of Si@TiO<sub>2</sub>@rGO composite with sandwich-like nanostructure as superior performance anodes for lithium ion batteries. *J. Alloys Compd.* 818:152884. doi: 10.1016/j.jallcom.2019.152884
- Fang, R., Xiao, W., Miao, C., Mei, P., Zhang, Y., Yan, X., et al. (2019). Fabrication of Si-SiO<sub>2</sub>@Fe/NC composite from industrial waste AlSiFe powders as high stability anodes for lithium ion batteries. *Electrochim. Acta* 324:134860. doi: 10.1016/j.electacta.2019.134860
- Fu, S., Ni, J., Xu, Y., Zhang, Q., and Li, L. (2016). Hydrogenation driven conductive Na<sub>2</sub>Ti<sub>3</sub>O<sub>7</sub> nanoarrays as robust binder-free anodes for sodium-ion batteries. *Nano Lett.* 16, 4544–4551. doi: 10.1021/acs.nanolett.6b01805
- Grosjean, C., Miranda, P. H., Perrin, M., and Poggi, P. (2012). Assessment of world lithium resources and consequences of their geographic distribution on the expected development of the electric vehicle industry. *Renew. Sust. Energ. Rev.* 16, 1735–1744. doi: 10.1016/j.rser.2011.11.023
- Guan, P., Zhou, L., Yu, Z., Sun, Y., Liu, Y., Wu, F., et al. (2020). Recent progress of surface coating on cathode materials for high-performance lithium-ion batteries. *J. Energy Chem.* 43, 220–235. doi: 10.1016/j.jechem.2019.08.022
- Guo, B., Liang, F., Zhang, B., and Gong, J. R. (2011). Graphene doping: a review. *Insci. J.* 1, 80–89. doi: 10.5640/insc.010280
- He, M., Walter, M., Kravchik, K. V., Erni, R., Widmer, R., and Kovalenko, M. V. (2015). Monodisperse SnSb nanocrystals for Li-ion and Na-ion battery anodes: synergy and dissonance between Sn and Sb. *Nanoscale* 7, 455–459. doi: 10.1039/C4NR05604C
- Hu, R., Waller, G. H., Wang, Y., Chen, Y., Yang, C., Zhou, W., et al. (2015). Cu<sub>6</sub>Sn<sub>5</sub>@SnO<sub>2</sub>-C nanocomposite with stable core/shell structure as a high reversible anode for Li-ion batteries. *Nano Energy* 18, 232–244. doi: 10.1016/j.nanoen.2015.10.037
- Huang, X., Cui, S., Chang, J., Hallac, P. B., Fell, C. R., Luo, Y., et al. (2015). A hierarchical tin/carbon composite as an anode for lithium-ion batteries with a long cycle life. *Angewandte. Chemie.* 127, 1510–1513. doi: 10.1002/ange.201409530
- Huang, Z., Hou, H., Zou, G., Chen, J., Zhang, Y., Liao, H., et al. (2016). 3D porous carbon encapsulated SnO<sub>2</sub> nanocomposite for ultrastable sodium ion batteries. *Electrochim. Acta* 214, 156–164. doi: 10.1016/j.electacta.2016.08.040
- Idota, Y., Kubota, T., Matsufuji, A., Maekawa, Y., and Miyasaka, T. (1997). Tin-based amorphous oxide: a high-capacity lithium-ion-storage material. *Science* 276, 1395–1397. doi: 10.1126/science.276.5317.1395
- Jiang, B., He, Y., Li, B., Zhao, S., Wang, S., He, Y.-B., et al. (2017). Polymer-templated formation of polydopamine-coated SnO<sub>2</sub> nanocrystals: anodes for cyclable lithium-ion batteries. *Angew. Chem. Inter. Ed.* 56, 1869–1872. doi: 10.1002/anie.201611160
- Jiang, Y., Guo, Y., Lu, W., Feng, Z., Xi, B., Kai, S., et al. (2017). Rationally incorporated MoS<sub>2</sub>/SnS<sub>2</sub> nanoparticles on graphene sheets for lithium-ion and sodium-ion batteries. *ACS Appl. Mater. Interfaces* 9, 27697–27706. doi: 10.1021/acsami.7b06572
- Jiang, Y., Song, D., Wu, J., Wang, Z., Huang, S., Xu, Y., et al. (2019). Sandwich-like SnS<sub>2</sub>/graphene/SnS<sub>2</sub> with expanded interlayer distance as high-rate lithium/sodium-ion battery anode materials. *ACS Nano* 13, 9100–9111. doi: 10.1021/acs.nano.9b03330
- Kepler, K. D., Vaughey, J. T., and Thackeray, M. M. (1999). Copper-tin anodes for rechargeable lithium batteries: an example of the matrix effect in an intermetallic system. *J. Power Sources* 81–82, 383–387. doi: 10.1016/S0378-7753(99)00111-1
- Kim, C., Noh, M., Choi, M., Cho, J., and Park, B. (2005). Critical size of a nano SnO<sub>2</sub> electrode for Li-secondary battery. *Chem. Mater.* 17, 3297–3301. doi: 10.1021/cm048003o
- Kim, H. S., Chung, Y. H., Kang, S. H., and Sung, Y.-E. (2009). Electrochemical behavior of carbon-coated SnS<sub>2</sub> for use as the anode in lithium-ion batteries. *Electrochim. Acta* 54, 3606–3610. doi: 10.1016/j.electacta.2009.01.030

- Kim, T.-H., Park, J.-S., Chang, S. K., Choi, S., Ryu, J. H., and Song, H.-K. (2012). The current move of lithium ion batteries towards the next phase. *Adv. Energy Mater.* 2, 860–872. doi: 10.1002/aenm.201200028
- Kim, T.-J., Kim, C., Son, D., Choi, M., and Park, B. (2007). Novel SnS<sub>2</sub>-nanosheet anodes for lithium-ion batteries. *J. Power Sources* 167, 529–535. doi: 10.1016/j.jpowsour.2007.02.040
- Kim, W.-S., Hwa, Y., Jeun, J.-H., Sohn, H.-J., and Hong, S.-H. (2013). Synthesis of SnO<sub>2</sub> nano hollow spheres and their size effects in lithium ion battery anode application. *J. Power Sources* 225, 108–112. doi: 10.1016/j.jpowsour.2012.10.030
- Kim, Y., Kim, Y., Choi, A., Woo, S., Mok, D., Choi, N.-S., et al. (2014). Tin phosphide as a promising anode material for Na-ion batteries. *Adv. Mater.* 26, 4139–4144. doi: 10.1002/adma.201305638
- Kou, Z., Miao, C., Mei, P., Zhang, Y., Yan, X., Jiang, Y., et al. (2019). Enhancing the cycling stability of all-solid-state lithium-ion batteries assembled with Li<sub>1.3</sub>Al<sub>0.3</sub>Ti<sub>1.7</sub>(PO<sub>4</sub>)<sub>3</sub> solid electrolytes prepared from precursor solutions with appropriate pH values. *Ceram. Int.* doi: 10.1016/j.ceramint.2019.12.229
- Lan, D., Wang, W., Shi, L., Huang, Y., Hu, L., and Li, Q. (2017). Phase pure Sn<sub>4</sub>P<sub>3</sub> nanotops by solution-liquid-solid growth for anode application in sodium ion batteries. *J. Mater. Chem. A* 5, 5791–5796. doi: 10.1039/C6TA10685D
- Larcher, D., Beaulieu, L. Y., Macneil, D. D., and Dahn, J. R. (2000). *In situ* X-ray study of the electrochemical reaction of Li with η<sup>-</sup>-Cu<sub>6</sub>Sn<sub>5</sub>. *J. Electrochem. Soc.* 147, 1658–1662. doi: 10.1149/1.1393413
- Lee, K. T., Jung, Y. S., and Oh, S. M. (2003). Synthesis of tin-encapsulated spherical hollow carbon for anode material in lithium secondary batteries. *J. Am. Chem. Soc.* 125, 5652–5653. doi: 10.1021/ja0345524
- Lefebvre, I., Lannoo, M., Moubtassim, M. E., Fourcade, J. O., and Jumas, J. C. (1997). Lithium insertion in three-dimensional tin sulfides. *Chem. Mater.* 9, 2805–2814. doi: 10.1021/cm970139h
- Li, D., and Kaner, R. B. (2008). Graphene-based materials. *Science* 320, 1170–1171. doi: 10.1126/science.1158180
- Li, J., Xu, X., Luo, Z., Zhang, C., Yu, X., Zuo, Y., et al. (2019). Compositionally tuned Ni<sub>x</sub>Sn alloys as anode materials for lithium-ion and sodium-ion batteries with a high pseudocapacitive contribution. *Electrochim. Acta* 304, 246–254. doi: 10.1016/j.electacta.2019.02.098
- Li, L., Zheng, Y., Zhang, S., Yang, J., Shao, Z., and Guo, Z. (2018). Recent progress on sodium ion batteries: potential high-performance anodes. *Energy Environ. Sci.* 11, 2310–2340. doi: 10.1039/C8EE01023D
- Li, M.-Y., Liu, C.-L., Shi, M.-R., and Dong, W.-S. (2011). Nanostructure Sn-Co-C composite lithium ion battery electrode with unique stability and high electrochemical performance. *Electrochim. Acta* 56, 3023–3028. doi: 10.1016/j.electacta.2010.12.102
- Li, R., Xiao, W., Miao, C., Fang, R., Wang, Z., and Zhang, M. (2019). Sphere-like SnO<sub>2</sub>/TiO<sub>2</sub> composites as high-performance anodes for lithium ion batteries. *Ceram. Int.* 45, 13530–13535. doi: 10.1016/j.ceramint.2019.04.059
- Li, Z., Ding, J., and Mitlin, D. (2015). Tin and tin compounds for sodium ion battery anodes: phase transformations and performance. *Acc. Chem. Res.* 48, 1657–1665. doi: 10.1021/acs.accounts.5b00114
- Lin, Y.-M., Abel, P. R., Gupta, A., Goodenough, J. B., Heller, A., and Mullins, C. B. (2013). Sn-Cu nanocomposite anodes for rechargeable sodium-ion batteries. *ACS Appl. Mater. Interfaces* 5, 8273–8277. doi: 10.1021/am4023994
- Liu, D., Fan, X., Li, Z., Liu, T., Sun, M., Qian, C., et al. (2019). A cation/anion co-doped Li<sub>1.12</sub>Na<sub>0.08</sub>Ni<sub>0.2</sub>Mn<sub>0.6</sub>O<sub>1.95</sub>F<sub>0.05</sub> cathode for lithium ion batteries. *Nano Energy* 58, 786–796. doi: 10.1016/j.nanoen.2019.01.080
- Liu, H., Li, W., Shen, D., Zhao, D., and Wang, G. (2015). Graphitic carbon conformal coating of mesoporous TiO<sub>2</sub> hollow spheres for high-performance lithium ion battery anodes. *J. Am. Chem. Soc.* 137, 13161–13166. doi: 10.1021/jacs.5b08743
- Liu, J., Kopold, P., Wu, C., Van Aken, P. A., Maier, J., and Yu, Y. (2015). Uniform yolk-shell Sn<sub>4</sub>P<sub>3</sub>@C nanospheres as high-capacity and cycle-stable anode materials for sodium-ion batteries. *Energy Environ. Sci.* 8, 3531–3538. doi: 10.1039/C5EE02074C
- Liu, J., Wen, Y., Van Aken, P. A., Maier, J., and Yu, Y. (2014). Facile synthesis of highly porous Ni-Sn intermetallic microcages with excellent electrochemical performance for lithium and sodium storage. *Nano Lett.* 14, 6387–6392. doi: 10.1021/nl5028606
- Liu, L., Xie, F., Lyu, J., Zhao, T., Li, T., and Choi, B. G. (2016). Tin-based anode materials with well-designed architectures for next-generation lithium-ion batteries. *J. Power Sources* 321, 11–35. doi: 10.1016/j.jpowsour.2016.04.105
- Liu, Y., Fan, X., Zhang, Z., Wu, H.-H., Liu, D., Dou, A., et al. (2019). Enhanced electrochemical performance of Li-rich layered cathode materials by combined Cr doping and LiAlO<sub>2</sub> coating. *ACS Sustain. Chem. Eng.* 7, 2225–2235. doi: 10.1021/acssuschemeng.8b04905
- Liu, Y., Kang, H., Jiao, L., Chen, C., Cao, K., Wang, Y., et al. (2014). Exfoliated-SnS<sub>2</sub> restacked on graphene as high-capacity, high-rate, and long-cycle life anode for sodium ion batteries. *Nanoscale* 7, 1325–1332. doi: 10.1039/C4NR05106H
- Luo, B., Qiu, T., Ye, D., Wang, L., and Zhi, L. (2016). Tin nanoparticles encapsulated in graphene backboned carbonaceous foams as high-performance anodes for lithium-ion and sodium-ion storage. *Nano Energy* 22, 232–240. doi: 10.1016/j.nanoen.2016.02.024
- Luo, W., Shen, F., Bommier, C., Zhu, H., Ji, X., and Hu, L. (2016). Na-ion battery anodes: materials and electrochemistry. *Acc. Chem. Res.* 49, 231–240. doi: 10.1021/acs.accounts.5b00482
- Momma, T., Shiraishi, N., Yoshizawa, A., Osaka, T., Gedanken, A., Zhu, J., et al. (2001). SnS<sub>2</sub> anode for rechargeable lithium battery. *J. Power Sources* 97, 198–200. doi: 10.1016/S0378-7753(01)00723-6
- Morales, J., Perez-Vicente, C., and Tirado, J. L. (1992). Chemical and electrochemical lithium intercalation and staging in 2H-SnS<sub>2</sub>. *Solid State Ion.* 51, 133–138. doi: 10.1016/0167-2738(92)90190-Z
- Nayak, P. K., Yang, L., Brehm, W., and Adelhelm, P. (2018). From lithium-ion to sodium-ion batteries: advantages, challenges, and surprises. *Angew. Chem. Int. Ed.* 57, 102–120. doi: 10.1002/anie.201703772
- Nie, Y., Xiao, W., Miao, C., Xu, M., and Wang, C. (2020). Effect of calcining oxygen pressure gradient on properties of LiNi<sub>0.8</sub>Co<sub>0.15</sub>Al<sub>0.05</sub>O<sub>2</sub> cathode materials for lithium ion batteries. *Electrochim. Acta* 334:135654. doi: 10.1016/j.electacta.2020.135654
- Palomares, V., Serras, P., Villaluenga, I., Hueso, K. B., Carretero-González, J., and Rojo, T. (2012). Na-ion batteries, recent advances and present challenges to become low cost energy storage systems. *Energy Environ. Sci.* 5, 5884–5901. doi: 10.1039/c2ee02781j
- Pan, H., Hu, Y.-S., and Chen, L. (2013). Room-temperature stationary sodium-ion batteries for large-scale electric energy storage. *Energy Environ. Sci.* 6, 2338–2360. doi: 10.1039/c3ee40847g
- Park, J.-W., and Park, C.-M. (2015). A fundamental understanding of Li insertion/extraction behaviors in SnO and SnO<sub>2</sub>. *J. Electrochem. Soc.* 162, A2811–A2816. doi: 10.1149/2.0891514jes
- Park, M.-G., Lee, D.-H., Jung, H., Choi, J.-H., and Park, C.-M. (2018). Sn-based nanocomposite for Li-ion battery anode with high energy density, rate capability, and reversibility. *ACS Nano* 12, 2955–2967. doi: 10.1021/acsnano.8b00586
- Park, M.-S., Wang, G.-X., Kang, Y.-M., Wexler, D., Dou, S.-X., and Liu, H.-K. (2007). Preparation and electrochemical properties of SnO<sub>2</sub> nanowires for application in lithium-ion batteries. *Angew. Chem. Int. Ed.* 46, 750–753. doi: 10.1002/anie.200603309
- Qian, J., Xiong, Y., Cao, Y., Ai, X., and Yang, H. (2014). Synergistic Na-storage reactions in Sn<sub>4</sub>P<sub>3</sub> as a high-capacity, cycle-stable anode of Na-ion batteries. *Nano Lett.* 14, 1865–1869. doi: 10.1021/nl404637q
- Qin, J., He, C., Zhao, N., Wang, Z., Shi, C., Liu, E.-Z., et al. (2014). Graphene networks anchored with Sn@Graphene as lithium ion battery anode. *ACS Nano* 8, 1728–1738. doi: 10.1021/nn406105n
- Qin, J., Liu, D., Zhang, X., Zhao, N., Shi, C., Liu, E.-Z., et al. (2017). One-step synthesis of SnCo nano confined in hierarchical carbon nanostructures for lithium ion battery anode. *Nanoscale* 9, 15856–15864. doi: 10.1039/C7NR04786f
- Read, J., Foster, D., Wolfenstine, J., and Behl, W. (2001). SnO<sub>2</sub>-carbon composites for lithium-ion battery anodes. *J. Power Sources* 96, 277–281. doi: 10.1016/S0378-7753(00)00569-3
- Ren, W., Zhang, H., Guan, C., and Cheng, C. (2018). SnS<sub>2</sub> nanosheets arrays sandwiched by N-doped carbon and TiO<sub>2</sub> for high-performance Na-ion storage. *Green Energy Environ.* 3, 42–49. doi: 10.1016/j.gee.2017.09.005
- Ren, Y., Wang, J., Huang, X., and Ding, J. (2017). Three-dimensional SnS<sub>2</sub> flowers/carbon nanotubes network: extraordinary rate capacity for sodium-ion battery. *Mater. Lett.* 186, 57–61. doi: 10.1016/j.matlet.2016.09.089
- Saadeddin, I., Hilal, H. S., Pecquenard, B., Marcus, J., Mansouri, A., Labrugere, C., et al. (2006). Simultaneous doping of Zn and Sb in SnO<sub>2</sub>

- ceramics: enhancement of electrical conductivity. *Solid State Sci.* 8, 7–13. doi: 10.1016/j.solidstatesciences.2005.09.002
- Slater, M. D., Kim, D., Lee, E., and Johnson, C. S. (2013). Sodium-ion batteries. *Adv. Funct. Mater.* 23, 947–958. doi: 10.1002/adfm.201200691
- Song, H. S., Li, S. L., Gao, L., Xu, Y., Ueno, K., Tang, J., et al. (2013). High-performance top-gated monolayer SnS<sub>2</sub> field-effect transistors and their integrated logic circuits. *Nanoscale* 5, 9666–9670. doi: 10.1039/c3nr01899g
- Stevens, D. A., and Dahn, J. R. (2000). High capacity anode materials for rechargeable sodium-ion batteries. *J. Electrochem. Soc.* 147, 1271–1273. doi: 10.1149/1.1393348
- Su, D., Ahn, H.-J., and Wang, G. (2013). SnO<sub>2</sub>@graphene nanocomposites as anode materials for Na-ion batteries with superior electrochemical performance. *Chem. Commun.* 49, 3131–3133. doi: 10.1039/c3cc40448j
- Sun, L., Ma, T., Zhang, J., Guo, X., Yan, C., and Liu, X. (2019). Double-shelled hollow carbon spheres confining tin as high-performance electrodes for lithium ion batteries. *Electrochim. Acta* 321:134672. doi: 10.1016/j.electacta.2019.134672
- Takamura, T., Suzuki, J., Yamada, C., Sumiya, K., and Sekine, K. (1999). Metal film deposition on carbon anodes for high rate charge–discharge of Li-ion batteries. *Surf. Eng.* 15, 225–229. doi: 10.1179/026708499101516560
- Tamura, N., Fujimoto, M., Kamino, M., and Fujitani, S. (2004). Mechanical stability of Sn-Co alloy anodes for lithium secondary batteries. *Electrochim. Acta* 49, 1949–1956. doi: 10.1016/j.electacta.2003.12.024
- Tarascon, J. M., and Armand, M. (2010). “Issues and challenges facing rechargeable lithium batteries,” in *Materials For Sustainable Energy*, ed D. Vincent (London, UK; Singapore: Macmillan Publishers Ltd; World Scientific), 171–179. doi: 10.1142/9789814317665\_0024
- Thangaraju, B., and Kaliannan, P. (2000). Spray pyrolytic deposition and characterization of SnS and SnS<sub>2</sub> thin films. *J. Phys. D Appl. Phys.* 33, 1054–1059. doi: 10.1088/0022-3727/33/9/304
- Tian, Q., Zhang, Z., Yang, L., and Hirano, S.-I. (2014). Encapsulation of SnO<sub>2</sub> nanoparticles into hollow TiO<sub>2</sub> nanowires as high performance anode materials for lithium ion batteries. *J. Power Sources* 253, 9–16. doi: 10.1016/j.jpowsour.2013.12.049
- Todd, A. D. W., Dunlap, R. A., and Dahn, J. R. (2007). Mössbauer effect studies of sputter-deposited tin-cobalt and tin-cobalt-carbon alloys. *J. Alloys Compd.* 443, 114–120. doi: 10.1016/j.jallcom.2007.06.030
- Trahey, L., Vaughey, J. T., Kung, H. H., and Thackeray, M. M. (2009). High-capacity, microporous Cu<sub>6</sub>Sn<sub>5</sub>-Sn anodes for Li-ion batteries. *J. Electrochem. Soc.* 156, A385–A389. doi: 10.1149/1.3094033
- Trifonova, A., Wachtler, M., Winter, M., and Besenhard, J. O. (2002). Sn-Sb and Sn-Bi alloys as anode materials for lithium-ion batteries. *Ionics* 8, 321–328. doi: 10.1007/BF02376044
- Uchiyama, H., Hosono, E., Honma, I., Zhou, H., and Imai, H. (2008). A nanoscale meshed electrode of single-crystalline SnO for lithium-ion rechargeable batteries. *Electrochem. Commun.* 10, 52–55. doi: 10.1016/j.elecom.2007.10.018
- Wang, G., Peng, J., Zhang, L., Zhang, J., Dai, B., Zhu, M., et al. (2015). Two-dimensional SnS<sub>2</sub>@PANI nanoplates with high capacity and excellent stability for lithium-ion batteries. *J. Mater. Chem. A* 3, 3659–3666. doi: 10.1039/C4TA06384H
- Wang, J., Luo, C., Mao, J., Zhu, Y., Fan, X., Gao, T., et al. (2015). Solid-state fabrication of SnS<sub>2</sub>/C nanospheres for high-performance sodium ion battery anode. *ACS Appl. Mater. Interfaces* 7, 11476–11481. doi: 10.1021/acsami.5b02413
- Wang, Y.-Q., Gu, L., Guo, Y.-G., Li, H., He, X.-Q., Tsukimoto, S., et al. (2012). Rutile-TiO<sub>2</sub> nanocoating for a high-rate Li<sub>4</sub>Ti<sub>5</sub>O<sub>12</sub> anode of a lithium-ion battery. *J. Am. Chem. Soc.* 134, 7874–7879. doi: 10.1021/ja301266w
- Wang, Z., Kou, Z., Miao, C., and Xiao, W. (2019). Improved performance all-solid-state electrolytes with high compacted density of monodispersed spherical Li<sub>1.3</sub>Al<sub>0.3</sub>Ti<sub>1.7</sub>(PO<sub>4</sub>)<sub>3</sub> particles. *Ceram. Int.* 45, 14469–14473. doi: 10.1016/j.ceramint.2019.04.192
- Wen, L., Li, F., and Cheng, H.-M. (2016). Carbon nanotubes and graphene for flexible electrochemical energy storage: from materials to devices. *Adv. Mater.* 28, 4306–4337. doi: 10.1002/adma.201504225
- Wen, Z., Cao, J., Gu, Z., Xu, X., Zhang, F., and Lin, Z. (2008). Research on sodium sulfur battery for energy storage. *Solid State Ion.* 179, 1697–1701. doi: 10.1016/j.ssi.2008.01.070
- Wu, L., Shi, S., Zhang, X., Yang, Y., Liu, J., Tang, S., et al. (2018). Room-temperature pre-reduction of spinning solution for the synthesis of Na<sub>3</sub>V<sub>2</sub>(PO<sub>4</sub>)<sub>3</sub>/C nanofibers as high-performance cathode materials for Na-ion batteries. *Electrochim. Acta* 274, 233–241. doi: 10.1016/j.electacta.2018.04.122
- Wu, L., Zheng, J., Wang, L., Xiong, X., Shao, Y., Wang, G., et al. (2019). PPy-encapsulated SnS<sub>2</sub> nanosheets stabilized by defects on a TiO<sub>2</sub> support as a durable anode material for lithium-ion batteries. *Angew. Chem. Int. Ed.* 58, 811–815. doi: 10.1002/anie.201811784
- Wu, Y., Nie, P., Wu, L., Dou, H., and Zhang, X. (2018). 2D MXene/SnS<sub>2</sub> composites as high-performance anodes for sodium ion batteries. *Chem. Eng. J.* 334, 932–938. doi: 10.1016/j.cej.2017.10.007
- Xia, L., Wang, S., Liu, G., Ding, L., Li, D., Wang, H., et al. (2016). Flexible SnO<sub>2</sub>/N-doped carbon nanofiber films as integrated electrodes for lithium-ion batteries with superior rate capacity and long cycle life. *Small* 12, 853–859. doi: 10.1002/smll.201503315
- Xiao, L., Cao, Y., Xiao, J., Wang, W., Kovarik, L., Nie, Z., et al. (2012). High capacity, reversible alloying reactions in SnSb/C nanocomposites for Na-ion battery applications. *Chem. Commun.* 48, 3321–3323. doi: 10.1039/c2cc17129e
- Xiao, W., Wang, Z., Zhang, Y., Fang, R., Yuan, Z., Miao, C., et al. (2018). Enhanced performance of P(VDF-HFP)-based composite polymer electrolytes doped with organic-inorganic hybrid particles PMMA-ZrO<sub>2</sub> for lithium ion batteries. *J. Power Sources* 382, 128–134. doi: 10.1016/j.jpowsour.2018.02.012
- Xin, S., Yin, Y.-X., Guo, Y.-G., and Wan, L.-J. (2014). A high-energy room-temperature sodium-sulfur battery. *Adv. Mater.* 26, 1261–1265. doi: 10.1002/adma.201304126
- Xu, Y., Zhu, Y., Liu, Y., and Wang, C. (2013). Electrochemical performance of porous carbon/tin composite anodes for sodium-ion and lithium-ion batteries. *Adv. Energy Mater.* 3, 128–133. doi: 10.1002/aenm.201200346
- Xue, L., Fu, Z., Yao, Y., Huang, T., and Yu, A. (2010). Three-dimensional porous Sn-Cu alloy anode for lithium-ion batteries. *Electrochim. Acta* 55, 7310–7314. doi: 10.1016/j.electacta.2010.07.015
- Yabuuchi, N., Kubota, K., Dahbi, M., and Komaba, S. (2014). Research development on sodium-ion batteries. *Chem. Rev.* 114, 11636–11682. doi: 10.1021/cr500192f
- Yang, J., Wachtler, M., Winter, M., and Besenhard, J. O. (1999). Sub-microcrystalline Sn and Sn-SnSb powders as lithium storage materials for lithium-ion batteries. *Electrochem. Solid-State Lett.* 2, 161–163. doi: 10.1149/1.1390769
- Yang, S., Yue, W., Zhu, J., Ren, Y., and Yang, X. (2013). Graphene-based mesoporous SnO<sub>2</sub> with enhanced electrochemical performance for lithium-ion batteries. *Adv. Funct. Mater.* 23, 3570–3576. doi: 10.1002/adfm.201203286
- Ying, H., and Han, W.-Q. (2017). Metallic Sn-based anode materials: application in high-performance lithium-ion and sodium-ion batteries. *Adv. Sci.* 4:1700298. doi: 10.1002/advs.201700298
- Yoon, S., Lee, J.-M., Kim, H., Im, D., Doo, S.-G., and Sohn, H.-J. (2009). An Sn-Fe/carbon nanocomposite as an alternative anode material for rechargeable lithium batteries. *Electrochim. Acta* 54, 2699–2705. doi: 10.1016/j.electacta.2008.11.060
- Yuan, Z., Dong, L., Gao, Q., Huang, Z., Wang, L., Wang, G., et al. (2018). SnSb alloy nanoparticles embedded in N-doped porous carbon nanofibers as a high-capacity anode material for lithium-ion batteries. *J. Alloys Compd.* 777, 775–783. doi: 10.1016/j.jallcom.2018.10.295
- Zhang, H.-X., Feng, C., Zhai, Y.-C., Jiang, K., Li, Q., and Fan, S.-S. (2009). Cross-stacked carbon nanotube sheets uniformly loaded with SnO<sub>2</sub> nanoparticles: a novel binder-free and high-capacity anode material for lithium-ion batteries. *Adv. Mater.* 21, 2299–2304. doi: 10.1002/adma.200802290
- Zhang, W.-J. (2011). A review of the electrochemical performance of alloy anodes for lithium-ion batteries. *J. Power Sources* 196, 13–24. doi: 10.1016/j.jpowsour.2010.07.020
- Zhao, K., Zhang, L., Xia, R., Dong, Y., Xu, W., Niu, C., et al. (2016). SnO<sub>2</sub> quantum dots@graphene oxide as a high-rate and long-life anode material for lithium-ion batteries. *Small* 12, 588–594. doi: 10.1002/smll.201502183
- Zhao, Y., Li, X., Yan, B., Li, D., Lawes, S., and Sun, X. (2015). Significant impact of 2D graphene nanosheets on large volume change tin-based anodes in lithium-ion batteries: a review. *J. Power Sources* 274, 869–884. doi: 10.1016/j.jpowsour.2014.10.008
- Zheng, P., Dai, Z., Zhang, Y., Dinh, K. N., Zheng, Y., Fan, H., et al. (2017). Scalable synthesis of SnS<sub>2</sub>/S-doped graphene composites for superior Li/Na-ion batteries. *Nanoscale* 9, 14820–14825. doi: 10.1039/C7NR06044K

- Zheng, Y., Zhou, T., Zhang, C., Mao, J., Liu, H., and Guo, Z. (2016). Boosted charge transfer in SnS/SnO<sub>2</sub> heterostructures: toward high rate capability for sodium-ion batteries. *Angew. Chem.* 128, 3469–3474. doi: 10.1002/ange.201510978
- Zhou, X., Bao, J., Dai, Z., and Guo, Y.-G. (2013a). Tin nanoparticles impregnated in nitrogen-doped graphene for lithium-ion battery anodes. *J. Phys. Chem. C* 117, 25367–25373. doi: 10.1021/jp409668m
- Zhou, X., Wan, L.-J., and Guo, Y.-G. (2013b). Binding SnO<sub>2</sub> nanocrystals in nitrogen-doped graphene sheets as anode materials for lithium-ion batteries. *Adv. Mater.* 25, 2152–2157. doi: 10.1002/adma.201300071
- Zhou, X., Yu, L., and Lou, X. W. (2016). Formation of uniform N-doped carbon-coated SnO<sub>2</sub> submicroboxes with enhanced lithium storage properties. *Adv. Energy Mater.* 6:1600451. doi: 10.1002/aenm.201600451
- Zhou, X., Yu, Y., Yang, J., Wang, H., Jia, M., and Tang, J. (2019). Cross-linking tin-based metal-organic frameworks with encapsulated silicon nanoparticles: high-performance anodes for lithium-ion batteries. *ChemElectroChem* 6, 2056–2063. doi: 10.1002/celec.201900235
- Zhu, H., Jia, Z., Chen, Y., Weadock, N., Wan, J., Vaaland, O., et al. (2013). Tin anode for sodium-ion batteries using natural wood fiber as a mechanical buffer and electrolyte reservoir. *Nano Lett.* 13, 3093–3100. doi: 10.1021/nl400998t
- Zhuo, L., Wu, Y., Wang, L., Yu, Y., Zhang, X., and Zhao, F. (2012). One-step hydrothermal synthesis of SnS<sub>2</sub>/graphene composites as anode material for highly efficient rechargeable lithium ion batteries. *RSC Advances* 2, 5084–5087. doi: 10.1039/c2ra00002d

**Conflict of Interest:** The authors declare that the research was conducted in the absence of any commercial or financial relationships that could be construed as a potential conflict of interest.

Copyright © 2020 Mou, Xiao, Miao, Li and Yu. This is an open-access article distributed under the terms of the Creative Commons Attribution License (CC BY). The use, distribution or reproduction in other forums is permitted, provided the original author(s) and the copyright owner(s) are credited and that the original publication in this journal is cited, in accordance with accepted academic practice. No use, distribution or reproduction is permitted which does not comply with these terms.